Trade study: Influence of different blade shape designs on forward flight and hovering performance of an isolated rotor

Martin Hollands[a], Manuel Keßler[a], Andree Altmikus[b], Ewald Krämer[a]

[a]*IAG, University of Stuttgart, Pfaffenwaldring 21, 70569 Stuttgart, Germany*
[b]*Eurocopter Deutschland GmbH, Willy-Messerschmitt-Straße, 81663 München, Germany*

Abstract

A trade study based on trimmed and coupled CFD simulations has been conducted. The influence of an increased chord length close to the blade tip on the performance of an isolated helicopter rotor in forward flight and in hovering condition is examined. At first a grid convergence study showed significant dependence of absolute values on the grid resolution, whereas relative values between different blade shape designs proved to be grid independent. Based on this study a positive effect of an augmented chord length on forward flight performance can be stated. Within a Design of Experiments approach four parameters related to blade-tip shape have been investigated to obtain information about the significance and the interaction of different parameters, as well as their effect on forward flight and hovering performance. Anhedral was dominant in both flight conditions. In hovering condition an increase of the anhedral had a positive effect, whereas in forward flight, blades with no anhedral showed best results. Yet an improvement in hover as well as in forward flight compared to a rectangularly shaped reference blade with parabolic tip section could be achieved.

Keywords: helicopter, trimmed and coupled isolated rotor, hover and forward flight performance, DoE, Taguchi

Nomenclature

Ψ	Rotor azimuth angle	[°]
θ_0	Collective pitch angle	[°]
θ_C	Cyclic pitch angle (cosine)	[°]
θ_S	Cyclic pitch angle (sine)	[°]
$\vec{F}_{2D}$	Aerodynamic loads and moments vector (BET)	
$\vec{F}_{3D}$	Aerodynamic loads and moments vector (CFD)	
C_P	Power coefficient	[-]
C_T	Thrust coefficient	[-]
$C_{P,P}$	Parasitic power coefficient	[-]
C_{Torque}	Torque coefficient	[-]
D	Rotor drag	[N]
e_a	Approximate relative error	[-]
e_{ext}	Extrapolated relative error	[-]
FM	Figure of Merit	[-]
GCI_{coarse}	Grid convergence index for coarser grid	[-]
GCI_{fine}	Grid convergence index for finer grid	[-]
L	Rotor lift	[N]
n	Number of rotor blades	[-]
P	Rotor power	[kW]
R	Rotor radius	[m]
r	Grid refinement factor	[-]
T	Period of one rotor revolution	[s]
X	Propulsive force of the rotor	[N]

Email address: `martin.hollands@iag.uni-stuttgart.de` (Martin Hollands)

Introduction

Modern helicopter designs, which achieve lower fuel consumption and noise emissions by reducing the blade tip Mach number, pose problems on the retreating blade, when operating at higher cruise speeds at the same time. As only a limited area in the outer section of the blade contributes to thrust generation, high pitch angles are required on the retreating side. Thus, it can be expected that an increased chord length in an area near the blade-tip has a positive effect on performance under these flight conditions. This effect is further investigated by means of Computational Fluid Dynamics (CFD) following a Design of Experiments (DoE) approach. The parametric study is performed by a simulation of an isolated rotor.

In order to perform trade studies efficiently with different geometric parameters the process chain shown in Figure 1 is used. The chain consists of a Python based tool

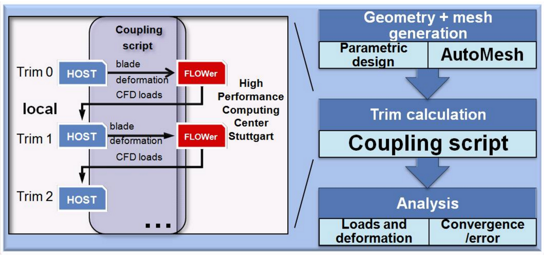

Figure 1: Process chain - trimmed simulation of an isolated rotor

which enables a parametric geometry design of helicopter rotor blades, an automatic grid generation process named *AutoMesh* [1] constructing high quality structured blade meshes and a Python based automatic coupling procedure. The fluid structure coupling is carried out by the structured finite volume RANS solver *FLOWer* developed by DLR [2, 3] on the CFD side and *HOST* from Eurocopter [4] on the structure side. Performing an aeroelastic simulation and trimming the rotor to a steady flight state is essential for the determination of power consumption in forward flight. Hence collective and cyclic pitch angles have to be trimmed to meet the following three objectives: thrust, pitching and rolling moments. Furthermore, deformation of the rotor blades is taken into account by coupling the flow solver with a Computational Structural Dynamics (CSD) method using a weak fluid-structure coupling scheme [5].

1. Numerical Models

1.1. Aerodynamic Modeling - CFD

The aerodynamic calculations have been carried out using the Finite-Volume flow solver *FLOWer*. The Reynolds-Averaged Navier-Stokes (RANS) equations are spatially discretized with second order central differences on a multi block-structured computational grid, using the third order dissipation scheme of Jameson [6]. For time discretization, an implicit dual time-stepping method by Jameson [7] has been used. Various overlapping grid structures can be realized applying the Chimera technique [8], which allows independent motion definitions of different grid structures. For convergence acceleration implicit residual smoothing as well as a multigrid approach with three grid levels are used.

1.2. Structural Modeling - CSD

Structural deformation as well as rotor trim is realized by the structure and flight mechanics code *HOST*. The elastic blade model consists of an Euler-Bernoulli beam discretized by rigid elements. Between those elements virtual joints allow rotations about all three axes. The Rayleigh-Ritz method is used to replace the multi degree of freedom system resulting from the rigid elements with a reduced number of modal shapes [9].

1.3. Fluid Structure Coupling

In order to account for fluid structure interaction in a steady forward flight or in steady hovering condition a weak fluid structure coupling method is used. As both cases are periodic problems, it is adequate to exchange periodic loads instead of an exchange within each timestep, as realized by a strong coupling method [5]. Trimming the rotor to the predefined objective is done within several iterations (see Figure 1, left-hand side). During the first step an initial state represented by the three pitch angles and the deformation of the rotor is determined. This *Trim 0* condition is obtained by *HOST* with internal blade element theory. Afterwards the corresponding CFD solution for this trim state is calculated with *FLOWer* and the periodic loads are transferred back to *HOST*. Within the next trim iteration the *HOST* load vector is composed of the internal two dimensional aerodynamics $\vec{F}_{2D}$ corrected with the CFD loads vector $\vec{F}^{n}_{3D}$ as follows:

$$\vec{F}^{n+1}_{HOST} = \vec{F}^{n+1}_{2D} + \left(\vec{F}^{n}_{3D} - \vec{F}^{n}_{2D}\right) \qquad (1)$$

1.4. Grid Generation

In order to obtain structured blade meshes with a good quality for arbitrary blade shapes an automatic grid generation tool *AutoMesh* was developed [1]. The main focus is on generating meshes with high quality concerning aspect ratio, skewness and growth rate. Therefore, a block topology was implemented that allows the boundary layer cells to surround the airfoil in an O-Block, whereas the outer region of the blade is designed in a C-Block shape. This technique reduces grid cells and at the same time improves grid quality compared to ordinary C-Block meshes especially at the blade tip and at the wake. Another prinicipal feature of *AutoMesh* is the ability to create blade meshes for various blade shapes with a constant topology and similar node distribution.

1.5. Process Chain

The process chain used for this parametric study is shown in Figure 1. At first the blade geometry is defined in a Python-based tool designed by Eurocopter Germany. An output to *AutoMesh* is generated to build up the blade mesh corresponding to the geometry. In the next step the fluid structure coupling procedure is controlled by Python scripts, which organize the file transfer between *HOST*, which is running on a local computer, and *FLOWer* running on the High Performance Computing Center Stuttgart (HLRS). After the trimming procedure is finished, the results can be evaluated based on *HOST* output data.

2. Computational Setup

Both, the rotor in forward flight and the hovering rotor are simulated using the described method of weak fluid structure coupling, acounting for fluid structure interaction and trimming the rotor to a predefined flight condition.

2.1. Forward Flight

In forward flight condition, the isolated rotor is calculated using a setup with five rotor blades, which are individually deformed and pitched. The Chimera grid system in Figure 2 shows the inclined rotor in the cartesian background mesh. The calculations were performed with a timestep equivalent to 1° of rotor revolution, while an average of 75 subiterations per timestep were used to achieve convergence of the solution.

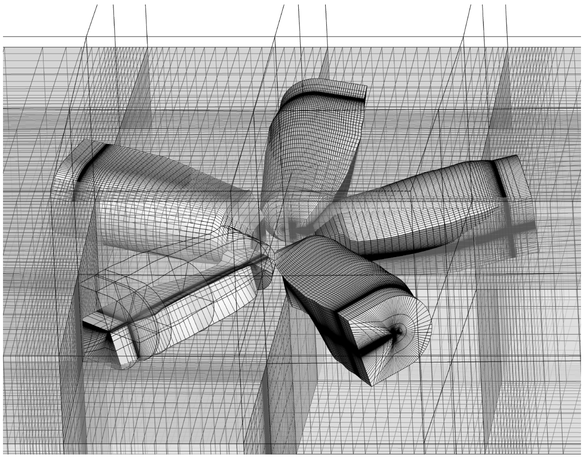

Figure 2: Grid system - forward flight, every second mesh line blanked.

2.2. Hover

For the hovering rotor, a periodic configuration with a single blade mesh is used (Figure 3). For every time step 50 subiterations have been computed. Starting with a timestep equivalent to 12°, the timestep is refined to 2° and to finally 1° in order to achieve a total of five rotor revolutions within each trim iteration. This takes into account that the rotor wake is convected only by induced velocity in hovering flight condition.

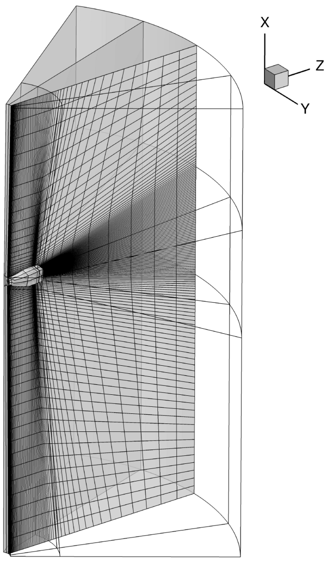

Figure 3: Grid system - hover

3. Convergence and Periodicity

3.1. Grid Convergence

Starting with an empirically good grid quality and 1.5 million cells for the blade mesh and a background mesh with 1 million cells the grid has been refined in two steps with a constant factor of 1.3 in each space dimension. As the number of grid points is limited to whole numbers and for three multi-grid levels a number divisible by four is required, an average refinement factor of $r_{32} = 1.306$ from the coarse (index 3) to the intermediate grid (index 2) and of $r_{21} = 1.299$ from intermediate to the fine grid (index 1) could be obtained. The boundary layer was resolved by 28 cells on the coarse, 36 cells on the intermediate and 48 cells on the fine grid. While the boundary layer thickness as well as the height of the first boundary layer cell was kept constant to a value assuring $y^+ < 1$, the cell growth rate within the boundary layer was refined. With these conditions a grid convergence study following [10, 11] was conducted to evaluate discretization errors with determination of the Grid Convergence Index (GCI). Results are summarized in Table 1 and 2 for the power coefficient C_P, the thrust coefficient C_T and the parasitic power coefficient $C_{P,P}$ representing a non-dimensional form of the propulsive force X. It is defined in [12] as:

$$C_{P,P} = \frac{X \cdot v_\infty}{\rho A (\Omega R)^3} \tag{2}$$

Table 1: Grid convergence index, C_P trimmed, C_T at initial trim

	$\Phi = C_P$ power coefficient $[10^{-4}]$	$\Phi = C_{P,P}$ parasitic power coefficient $[10^{-4}]$	$\Phi = C_T$ thrust coefficient (Trim 0) $[10^{-3}]$
Φ_1	7.651	3.616	7.332
Φ_2	7.767	3.639	7.312
Φ_3	7.993	3.677	7.207
Φ_{ext}	7.522	3.598	7.352
e_a^{21}	1.51%	0.54%	0.27%
e_{ext}^{21}	1.71%	0.61%	0.27%
GCI_{fine}^{12}	2.11%	0.76%	0.34%
GCI_{fine}^{23}	3.94%	1.43%	0.68%
GCI_{coarse}^{13}	7.69%	2.74%	1.39%

Table 2: Grid convergence index, for C_P, $C_{P,P}$ and C_T using the trim and deformation state of the fine grid solution on all three grid levels

	$\Phi = C_P$ $[10^{-4}]$	$\Phi = C_{P,P}$ $[10^{-4}]$	$\Phi = C_T$ $[10^{-3}]$
Φ_1	7.651	3.616	8.820
Φ_2	7.678	3.612	8.781
Φ_3	7.742	3.601	8.712
Φ_{ext}	7.631	3.619	8.869
e_a^{21}	0.35%	0.12%	0.43%
e_{ext}^{21}	0.26%	0.08%	0.56%
GCI_{fine}^{12}	0.32%	0.01%	0.70%
GCI_{fine}^{23}	0.75%	0.24%	1.25%
GCI_{coarse}^{13}	1.81%	0.61%	2.22%

The grid convergence index shows that there is still a considerable grid dependence of the solution, in terms of the rotor power coefficient after the rotor has been trimmed (Table 1). However, the error band includes not only the error of the CFD solution but also a deviation due to a different trim solution. The evaluation of the propulsive force shows less influence of the grid solution than the values related to rotor power. For estimating the error within the CFD calculation, an evaluation of the GCI was additionally done for the thrust coefficient of the initial trim iteration, where the deformation and the pitch angles given by *HOST* were identical (Table 1 last column). Furthermore two calculations with the same deformation as the last trim of the fine grid were performed on the coarse and the intermediate grid (Table 2). The error stays within an error-band of 2% for the coarse grid. For the thrust value the apparent order is slightly overestimated resulting in $r^p = 1.77$ which is 5% higher than the expected value of $r^p = 1.69$ for a second order accurate calculation. The value is even 40% off the expected value for C_P indicating that the solution is not within the asymptotic range. Yet for the GCI the evaluation of thrust values is more reliable as the integrated thrust is related only once to the radial node distribution. The GCI was calculated with a safety factor of 1.25 following the recommendation of Celic [10]. Using a more conservative safety factor of 3 as suggested by Roache [11] leads to an error-band of about 5% for the coarse grid solution. From the results of Table 1 and 2 it may also be seen that with a refinement of the grid the rotor thrust is increased while the power consumption of the rotor is reduced. In Figure 4 and 5 the difference of rotor thrust between the different grid solutions relative to the average thrust is shown. The deviation is within a range of 5 %. The differences can be related to a higher dissipation of vortices on coarser grids, as a similar structure can be found within the vortex visualization with the λ_2 criterion (Figure 6 and 7). In particular, small vortex filaments present on Figure 6 are completely dissipated on the coarse grid Figure 7. While the main vortices are preserved on the coarse grid, their strength is weaker than on the fine grid. This influence on rotor thrust

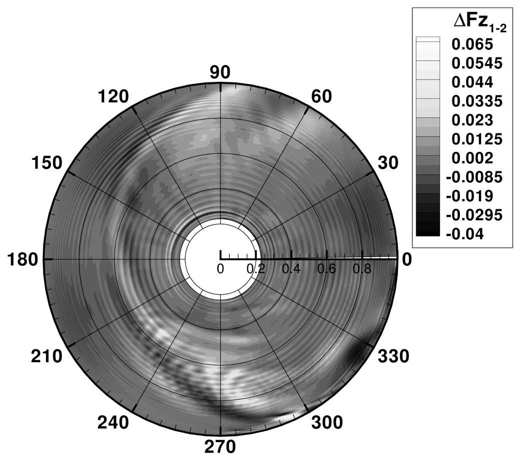

Figure 4: Dimensionless thrust difference: $\Delta F_{z,1-2}$ fine-intermediate grid

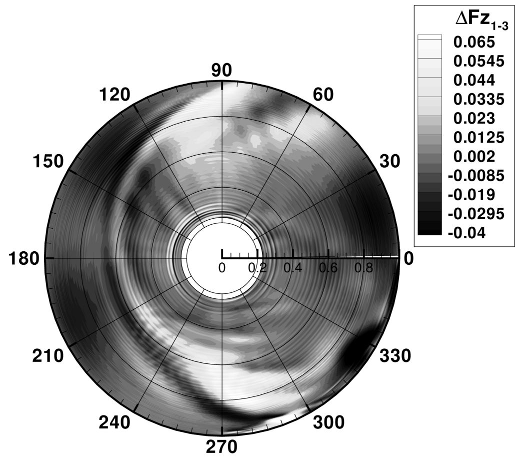

Figure 5: Dimensionless thrust difference $\Delta F_{z,1-3}$ fine-coarse grid

is also reflected by the resulting collective and cyclic pitch angles (Table 3). On the retreating blade higher pitch angles are required for the solution based on the coarser grid. Moreover an increase of the collective pitch angle can be stated. This explains the rise of power consumption when coarsening the grid. The grid convergence index and the related examination of the flow field shows a considerable dependence on the mesh resolution. With an error of about 4 % the intermediate grid appears as best choice concerning accuracy and computing effort.

Table 3: Collective and cyclic pitch angles

	fine	intermediate	coarse
θ_0	3.83°	3.93°	4.12°
θ_C	1.73°	1.74°	1.78°
θ_S	-10.55°	-10.64°	-10.81°

3.2. Periodicity

As for the weak coupling scheme periodic loads are required, CFD calculations should be performed until a periodic flow field is obtained. Therefore, an automatic determination of the periodicity by calculating the auto-correlation between two following periods of the aerodynamic loads has been implemented. With $\vec{F}^{(t)}_{3D}(\Psi, z/R)$ representing the aerodynamic loads at discrete points at the time t and $\overline{\vec{F}^{(t)}_{3D}}$ the mean over the rotor disk at that given time the functions G and H are defined as:

$$G = \vec{F}^{(t)}_{3D} - \overline{\vec{F}^{(t)}_{3D}} \tag{3}$$

$$H = \vec{F}^{(t+\frac{T}{n})}_{3D} - \overline{\vec{F}^{(t+\frac{T}{n})}_{3D}} \tag{4}$$

The normalized auto-correlation A is now given by the inner product:

$$A = \left\langle \frac{G}{\|G\|_2}, \frac{H}{\|H\|_2} \right\rangle \tag{5}$$

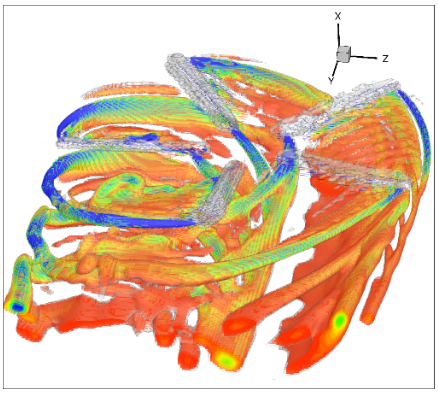

Figure 6: Vortex visualization with λ_2 criterion for fine grid.

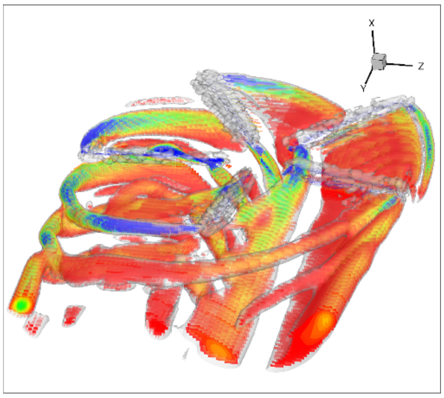

Figure 7: Vortex visualization with λ_2 criterion for coarse grid

A attains its maximum $A = 1$ when G and H are periodic. Thus, the correlation factor can be defined as $CF = 1 - A$. Figure 8 shows the results for a trim process of an isolated rotor in forward flight consisting of five trim iterations, where Ψ is the azimuth angle in degrees representing the CFD time step. The first correlation can be done after two periodic cycles which explains the gap of 144° between each trim iteration in Figure 8. The correspond-

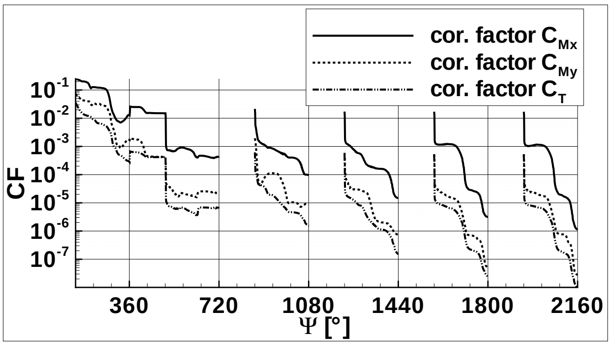

Figure 8: Correlation Factor over five trim iterations

ing trend of the rotor thrust in Figure 9 demonstrates that with a falling correlation factor CF (Figure 8) the trim objective converges to a constant value within each trim iteration. Furthermore, the pitch angles show the convergence of the trim after four to five trim iterations. This correlation

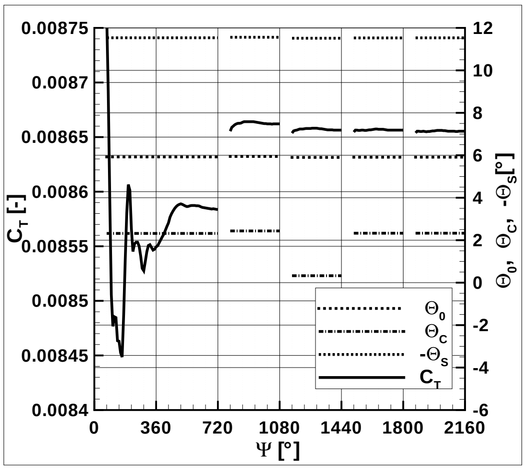

Figure 9: Thrust coefficient of aerodynamic loads over five trim iterations

factor serves two purposes. On the one hand it represents a suitables means of determining the periodicity of the loads vector and can thus be used as convergence criterion for monitoring. On the other hand it allows to specify a treshold by experience, for automatically changing to the next trim iterationstep. In Figure 10 the results for a trim with only 288° per trim iteration is shown. The correlation coefficient also converges to a value of 10^{-6} for the thrust coefficient, which indicates a good periodicity of the solution. Figure 11 proves that the thrust value converges within each trim iteration. A converged trim with a change of the pitch

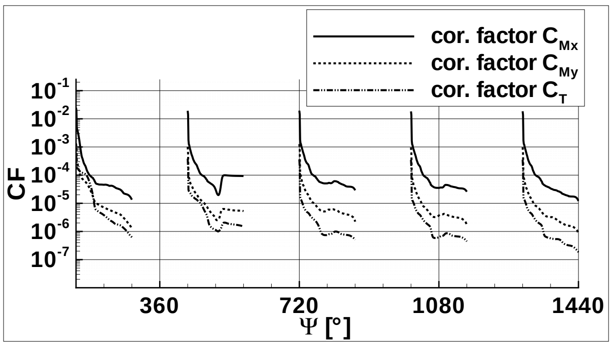

Figure 10: Correlation Factor over five ”288°-trim” iterations

angles below 0.01° is obtained after five trim iterations as before. Thus one rotor revolution of calculation time can be saved without a negative influence on the accuracy of the solution. Furthermore, it is shown that within the first trim iteration there is no need to achieve a fully converged solution as within the next iterations the trim converges as fast as in Figure 8, where two rotor revolutions have been used for the initial trim.

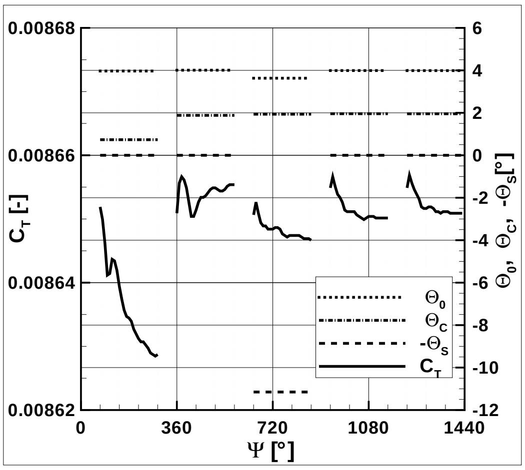

Figure 11: Thrust coefficient of aerodynamic loads over five ”288°”-trim iterations

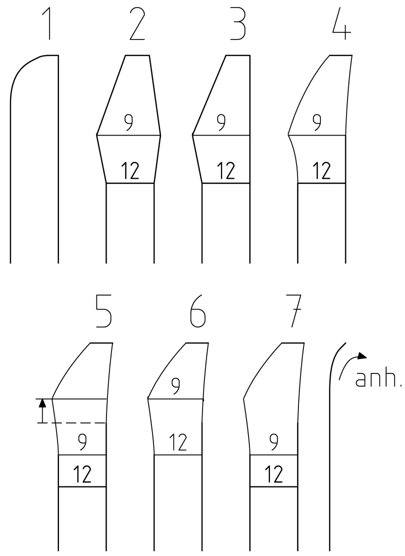

Figure 12: Examined blade shape parameters

4. Trade study

4.1. Comparison of Coarse and Intermediate Grid Solutions

Acounting for the grid dependence of the solution a first parametric study is conducted, examining the relative differences between different geometric blade shapes both on the coarse and the intermediate grid. The blade shape parameters are then further investigated in a second study. The GCI previously calculated represents a means for determining an error band for the calculation of absolute values. Yet, for optimization studies relative values are of importance. The question that remains is thus the behaviour of the error concerning relative values between different geometries. Consequently seven different geometrical variations have been selected (schematic Figure 12). Blade 1 is the reference blade, a rectangular blade shape with parabolic tip. For blade 2 the blade area near to the blade tip was increased at about $0.8\,R$, the numbers 9 and 12 indicate a change of the airfoil thickness. Blade 3 changes the azimuthal position of the maximum chord length, so that a straight trailing edge is obtained. Blade 4 has a curved leading edge. The position of the maximum chord length was moved outward in radial direction for blade 5, 6 and 7. Blade 6 varies the position of the airfoil change and finally blade 7 has an increased anhedral. All blades are designed to achieve the same thrust-weighted area. For each geometry a trimmed forward flight simulation has been evaluated on both intermediate and coarse grid.

4.1.1. Quality Criterion

In forward flight the power consumption is highly dependend on the attitude of the helicopter, therefore it is essential to trim the rotor to a steady flight position to evaluate its efficiency. As described above, the isolated rotor was trimmed to meet the objectives thrust, pitching and rolling-moment, while the pitch attitude of the rotor disk is kept constant. The following criterion is based on the assumption that the helicopter fuselage always has approximately the same parasitic drag which has to be overcome by rotor propulsive force X. While the thrust of all trimmed rotors is the same, X may vary with different rotor blade designs. Consequently it is essential not only to compare the power consumption represented by the power coefficient C_P, but also to include the propulsive force X in a quality criterion for a rotor in forward flight. A common means is to calculate the Lift over Drag L/D ratio for the rotor (as defined in [12] and also studied in [13]):

$$\frac{L}{D} = \frac{L}{\frac{P}{v_\infty} - X} \tag{6}$$

4.1.2. Results

The results of the quality criterion as well as the power coefficient for the seven configurations from Figure 12 is presented in Figure 13. The grid dependence of absolute values examined before is also present here with an almost constant offset between solutions of the coarse compared to those of the intermediate grid. Yet, the computational mesh has less influence on relative values. The qualitative trend between different geometries shows a good agreement on both grid solutions. Concerning the pitch angles obtained by trimming the rotor a similar behaviour can be stated (Figure 14). There is a slight increase of collective and sinusoidal pitch for the coarse grid and an almost equal behaviour of the cosine term of the cyclic pitch angle, so that there is an overall increase of pitch angle at the retreating side of the rotor. The good qualitative agreement found in Figures 13 and 14 indicates that for optimization problems the coarse grid solutions may still be adequate assuring that the examined geometrical changes can be resolved within the solution. Furthermore, it is essential for this study to use an identical grid topology within one grid level, in order to guarantee that the node distribution stays similar and is only changed within geometric necessity of different blade shape geometries.

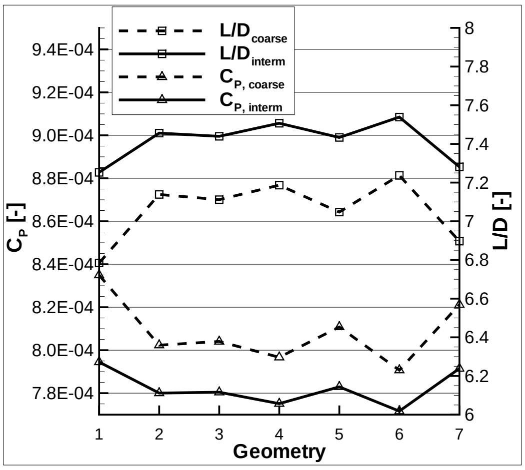

Figure 13: Quality criterion for forward flight on coarse and intermediate grids

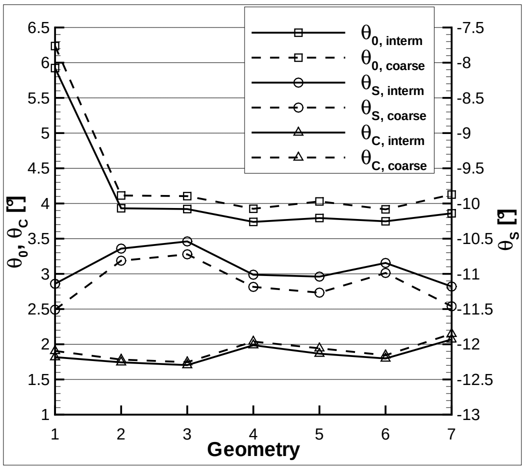

Figure 14: Pitch angles for forward flight on coarse and intermediate grids

4.2. DoE Approach

A further examination of the blade shape parameters of Figure 12 was done following the Taguchi approach [14, 15] for Design of Experiments (DoE). The geometric change between geometry 2 and 3 was excluded as the effect on forward flight performance was minor and thus the parameters could be reduced to four with three levels (Table 4). Within a full factorial experiment this leads to 81 designs which would have to be evaluated. The strength of the Taguchi approach is to reduce the numbers of experiments from in this case 81 to 9 by the selection of an L-9 orthogonal array. Furthermore, it offers the possibility to determine the optimum set of parameter levels and to conduct an analysis of variance (ANOVA) to identify the significance of different parameters. The orthogonal array is given in Table 5 as well as the corresponding responses for forward flight, L/D as previously defined and for hovering condition the Figure of Merit FM. Two results for each flight condition are given to account for the amount of uncertainty remaining between the last (n) and the second to last ($n-1$) trim iteration. The comparison of the results

Table 4: Factor levels

	factor	Level 1	2	3
A	Geometry LE	both linear	both curved	forward curved backward linear
B	z/R-Position	original	-4%	+4%
C	Anhedral	5°	zero	doubled (parabolic shape)
D	Airfoil z/R	original	-4%	+4%

Table 5: Inner Array L-9

Exp.	Control factor A	B	C	D	Forward flight L/D_{n-1}	L/D_n	Hover FM_{n-1}	FM_n
1	1	1	1	1	7.137	7.139	0.7245	0.7244
2	1	2	2	2	7.294	7.294	0.7235	0.7242
3	1	3	3	3	6.955	6.950	0.7316	0.7315
4	2	1	2	3	7.306	7.305	0.7239	0.7238
5	2	2	3	1	6.970	6.967	0.7393	0.7391
6	2	3	1	2	7.050	7.048	0.7327	0.7331
7	3	1	3	2	6.980	6.980	0.7430	0.7429
8	3	2	1	3	7.158	7.155	0.7319	0.7321
9	3	3	2	1	7.328	7.325	0.7259	0.7259

for forward flight with $L/D = 6.784$ of the reference rotor confirms the positive effect of an increased chord length near the blade tip in forward flight. All configurations improve L/D by at least 2.4% and up to 7.6%. Configurations with an increased anhedral are less effective in forward flight. Yet, in hover the Figure of Merit is increased by 1%. Compared to $FM = 0.733$ of the reference blade in hover all configurations with a reduced anhedral (factor C level 1 and 2) reduce the Figure of Merit by about 1%.

In order to examine the interaction of different factors the corresponding quality criteria for hover and forward flight are indicated over their three levels in Figure 15 - 18. On the one hand, the development of different factors in forward flight condition can be compared to their development in hovering condition. Factors A, C and D have different and even contrary trends. In particular, the airfoil position and anhedral show a competitive effect on the effectiveness of a rotor in hover compared to the rotor in forward flight. On the other hand, a comparison between different factors also results in anti-synergetic interactions, as the trend varies qualitatively. Due to these interactions between different parameters further results and predictions of optimal parameter sets have to be dealt with care, as the effects may not be predicted correctly by the linear modelling and the influence of a single factor can not be seperated completely from accumulative effects of different factors.

The ANOVA results are given in Table 6 and 7. The most significant factor in hover is the anhedral (Factor

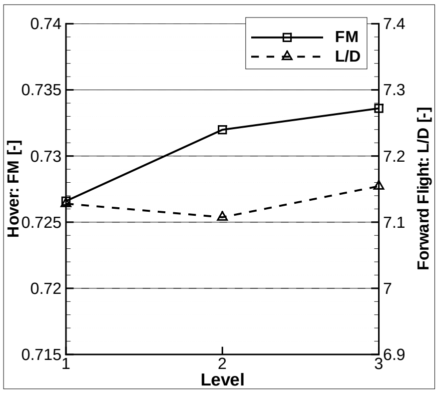

Figure 15: Factor A: Geometry LE for forward flight and hover

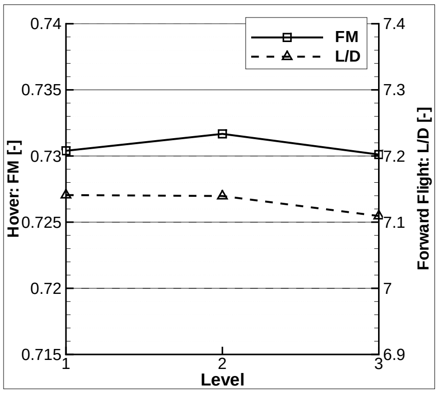

Figure 16: Factor B: z/R-Position for forward flight and hover

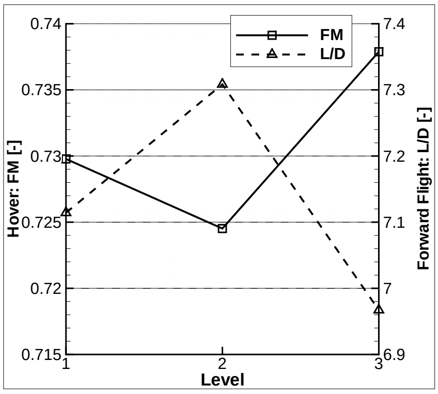

Figure 17: Factor C: Anhedral for forward flight and hover

C) with 70%. In forward flight it is even more dominant with almost 96%. In hover the geometry of the leading edge (Factor A) with 21% and the airfoil position with 7.6% are also significant while these factors play a minor role in forward flight. The important negative influence of an increased anhedral in forward flight can be explained by an area with negative thrust at the blade tip at an azimuth position of 100° – 150° (where 180° is the forward flight direction). This area is increased by introducing an anhedral to the blade tip as the local angle of attack gets

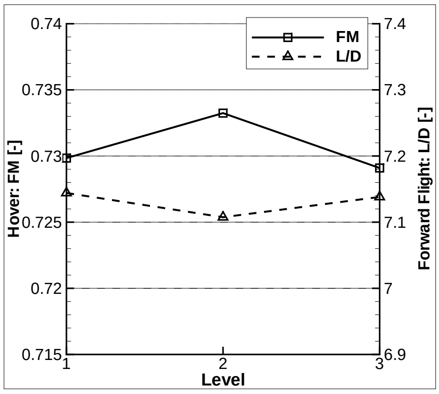

Figure 18: Factor D: Airfoil z/R for forward flight and hover

negative due to an increased flow from above through the rotor disc. In hover the anhedral has a positive influence on the convection of the blade tip vortex and leads to a reduced power consumption.

Table 6: ANOVA results for hover

	Sum of squares $[10^{-4}]$	DOF	Mean Square $[10^{-4}]$	Significance p [%]
A	1.62	2	0.81	20.9
B	0.08	2	0.04	1.1
C	5.44	2	2.72	70.4
D	0.59	2	0.29	7.6
error	0.001	9		
total	7.73	17		100

Table 7: ANOVA results for forward flight

	Sum of squares $[10^{-2}]$	DOF	Mean Square $[10^{-2}]$	Significance p [%]
A	0.664	2	0.332	1.8
B	0.384	2	0.192	1.0
C	35.16	2	17.58	95.8
D	0.463	2	0.231	1.2
error	0.001	9		
total	36.68	17		100

The optimum set of parameters for hover is (3, 2, 3, 2) with a predicted Figure of Merit of $FM_{opt,pre} = 0.744$. The actual calculated value of $FM_{opt,cal} = 0.7424$ corresponds well (error of 0.2%) with the prediction, yet Experiment 7 is at least on an equal level of the predicted optimal solution. The performance in forward flight is with $L/D = 7.02$ still 3% better than the reference blade but not among the best configurations. The verification of the optimum set (3, 1, 2, 1) for forward flight with $L/D_{opt,pre} = 7.356$ and $L/D_{opt,cal} = 7.299$ shows that a good solution is obtained.

However, it is not the best solution as Experiments 9 and 4 are better or at least on equal level. But concerning the error of the predicted with respect to the actual value of 0.8% a good accordance can also be found. With regards to the uncertainty of the solution due to mesh dependencies and convergence errors, it has to be stated that Experiment 9 and 4 are on an equal level to the predicted solution, as the difference of about 0.5% is certainly within the error-band of the solution. Thus the conclusion is that a valuable prediction of the optimal sets can be obtained from Taguchi approach although there are interactions between different factors. This can be explained by the dominance of factor C (anhedral), which has the largest influence on the effectiveness of the rotor in hover and in forward flight.

Finally, thrust distribution of the optimum solution for hover (index OH) and for forward flight (index OF) will be compared to the reference blade (index Ref). In Figure 19, 20 and 21 the thrust differences in forward flight show that for the new designs the thrust is increased at the outer region of the blade at an azimuth of $\Psi = 90° - 180°$, while a reduction of thrust at $\Psi = 60° - 90°$ as well as in the inner region of $\Psi = 90° - 180°$ is present. Furthermore, it is remarkable that on the retreating side thrust values are increased apart from the area close to the blade tip, where the blade area was reduced. At the same time the pitch angles are diminished (Table 8). On the retreating side the pitch angle is reduced by 3° for the optimum solution in forward flight and 2° for the optimum solution in hover so that the required thrust can be generated more efficiently with less power consumption of the rotor. Yet, the new designs lead to $2-4\%$ smaller values of propulsive force, which has also to be contemplated concerning the efficiency of the rotor.

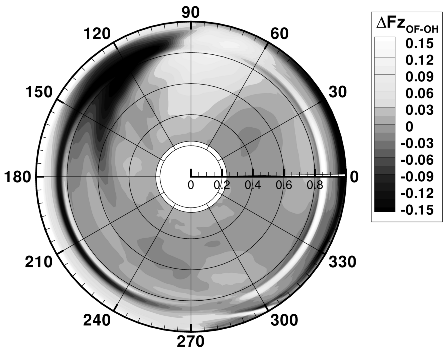

Figure 19: Dimensionless thrust difference in forward flight: $\Delta F_{OF,OH}$ (Optimum solution of forward flight) - (optimum hover)

For hover these three configurations are set in contrast with each other examining the local thrust coefficient as well as the torque coefficient defined as:

$$C_{Torque} = \frac{M_Z \Omega}{\rho A (\Omega R)^3} \tag{7}$$

In Figure 22 the trend of the thrust coefficient of the reference blade differs only slightly from that of configuration

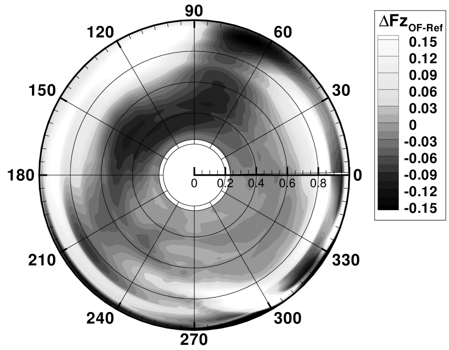

Figure 20: Dimensionless thrust difference in forward flight: $\Delta F_{OF,Ref}$ (Optimum solution of forward flight) - (reference blade)

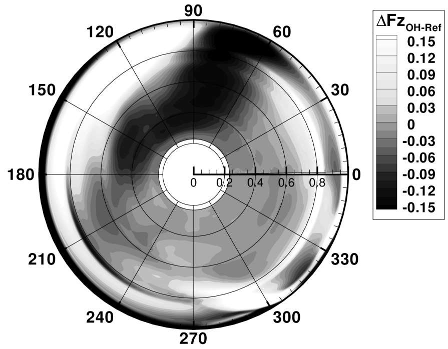

Figure 21: Dimensionless thrust difference in forward flight: $\Delta F_{OH,Ref}$ (Optimum solution of hover) - (reference blade)

Table 8: Collective and cyclic pitch angles for different geometries

	Ref	OF	OH
θ_0	6.24°	3.63°	3.90°
θ_C	1.91°	1.94°	2.46°
θ_S	-11.51°	-11.15°	-11.68°

OF, while configuration OH reduces the peak and thus approaches the curve closer to an ideal triangular thrust distribution. However, the local drag represented by C_{Torque} shows a negative effect of the forward and backward sweep leading to a peak of the local torque value. For configuration OH this effect is overcompensated by the reduced C_{Torque}-value close to the blade tip, leading to an increased Figure of Merit compared to the reference blade.

5. Conclusion

The influence of an increased chord length close to the blade tip on the effectiveness of an isolated rotor both in forward flight and hovering condition was examined. Trimmed and coupled simulations of an isolated rotor were conducted accounting for fluid structure interactions. A convergence criterion for the periodicity of the loads vector was introduced, offering the possibility to determine the initiation point of the next trim iteration.

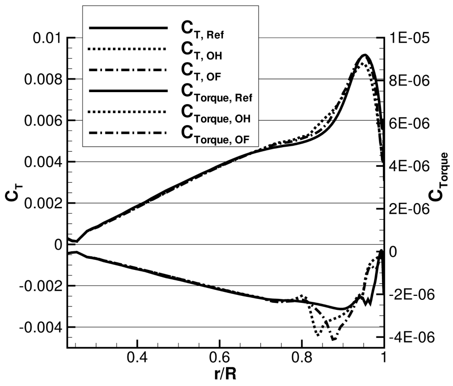

Figure 22: Thrust and torque coefficient in hover for optimum solutions in hover and forward flight and reference blade

At first the dependency of the solution on the mesh resolution has been examined on three different grid levels within a grid convergence study. While the error within a single trim iteration is rather small with 1.4% for the coarse grid, the cumulative error represented by the rotor power after a fully converged trim with several iterations showed an error band of 2% for the fine grid and a significant error band of 7.4% for the coarse grid. Yet in a second study comparing different geometries on the intermediate and the coarse grid solution a qualitatively good agreement on both grid levels could be stated, while absolute values showed a constant offset. Thus it was concluded that for a parametric study the coarse grid is still an adequate choice. It could also be shown that all configurations with an increased chord length close to the blade tip performed better in forward flight than the rectangularly shaped reference blade with parabolic tip section. The overall pitch angle and in particular the pitch angle on the retreating side of the rotor could be reduced leading to a lower power consumption. Finally, a parametric study based on a DoE approach was conducted to examine the effect of different geometric parameters on forward flight and hovering performance. While in forward flight all configurations improved the power consumption compared to the reference rotor, in hover the effect of an increased chord length is different. Some configurations showed a deterioration of the Figure of Merit of about 1%. Increasing the anhedral could compensate this effect and even lead to an improvement of the Figure of Merit of 1%. In forward flight on the contrary anhedral had a negative effect on the performance. Nevertheless, the best configuration in hover showed an increase in lift over drag of the rotor of 3%. The Taguchi method proved to be a reliable means for determining the significance of different parameters and their interaction. Though the basic assumption of the linear model that the effect of a factor can be separated from the effect of others was not fulfilled due to interactions of different factors, the predicted optimal sets showed good results. They were within an error band of 0.5% among the best configurations that have been examined.

As anhedral showed an important influence in hover and in forward flight, a further investigation by a more detailed parametrization of the geometric shape of a bended blade tip seems to be promising to achieve a greater improvement. In particular a multi-disciplinary approach to examine the competitive effect of anhedral on hover performance and on forward flight efficiency may help to find a compromise for both flight conditions.

Acknowledgments

The authors would like to thank the German Federal Ministry of Economy and Technology (BMWi) for its funding in the framework of FTEG-ECO-HC under grant 20H0803. We also like to acknowledge the support of the members of the aerodynamic department of Eurocopter for input of their practical experience.

References

1. Kranzinger P, Hollands M, Keßler M, Wagner S, Krämer E. "Generation and Verification of Meshes Used in Automatic Process Chains to Optimize Rotor Blades". In: *"50th AIAA Aerospace Sciences Meeting"*. Nashville, USA; 2012:[submitted].
2. Kroll N, Eisfeld B, Bleecke HM. "FLOWer". *Notes on Numerical Fluid Mechanics* 1999;71:58–68.
3. Schwarz TO. "Ein blockstrukturiertes Verfahren zur Simulation der Umströmung komplexer Konfigurationen". Universität Braunschweig , Germany: PhD thesis; 2005.
4. Benoit B, Dequin AM, Kampa K, von Grünhagen W, Basset PM, Gimonet B. "HOST, A General Helicopter Simulation Tool for Germany and France". Virginia Beach, Virginia USA; 2000:May 2–4.
5. Altmikus A, Wagner S, Beaumier P, Servera G. "A Comparison: Weak versus Strong Modular Coupling for Trimmed Aeroelastic Rotor Simulations". Montreal, Canada; 2002:697–710.
6. Jameson A, Schmidt W, Turkel W. "Numerical Solution of the Euler Equations by Finite Volume Methods using Runge-Kutta Time-Stepping Schemes". In: *AIAA 14th Fluid and Plasma Dynamic Conference*. Palo Alto, California, USA; 1981: 15.
7. Jameson A. "Time Dependent Calculations using Multigrid, with Applications to Unsteady Flows past Airfoils and Wings". In: *AIAA 10th Computational Fluid Dynamics Conference*. Honolulu, Hawaii, USA; 1991:91–1596.
8. Benek JA, Steger JL, Dougherty F, Buning PG. "Chimera: A grid-embedding technique". In: *NASA techdocs*. 19860022770; 1986:86N32242.
9. Dietz M. Simulation der Umströmung von Hubschrauberkonfigurationen unter Berücksichtigung von Strömungs-Struktur-Kopplung und Trimmung. Universität Stuttgart: PhD thesis; 2009.
10. Celik IB, Ghia U, Roache PJ, Freitas CJ, Coleman H, Raad PE. "Procedure for Estimation and Reporting of Uncertainty Due to Discretization in CFD Applications". *Journal of Fluids Engineering* 2008;130(7).
11. Roache PJ. "Quantification of Uncertainty in Computational Fluid Dynamics". *Annual Review of Fluid Mechanics* 1997;29:123–60.
12. Leishman JG. "Principles of Helicopter Aerodynamics". 2nd ed.; Cambridge Aerospace Series; 2006.
13. Altmikus A. "Criteria for Performance Assessment of Isolated Rotors in Forward Flight in Weakly Coupled CFD-CSD-Simulations". Tech. Rep.; Eurocopter Germany; 2010.
14. Taguchi G, Elsayed EA, Hsiang T. "Quality Engineering in Production Systems". Singapore: McGraw-Hill; 1989.
15. Klein B. "Versuchsplanung - DoE ". 2nd ed.; München: Oldenbourg; 2007.